JCTC Journal of Chemical Theory and Computation

pubs.acs.org/JCTC Article

Potential Energy Surfaces without Unphysical Discontinuities: The Coulomb Hole Plus Screened Exchange Approach

J. Arjan Berger,* Pierre-François Loos, and Pina Romaniello

Cite This: J. Chem. Theory Comput. 2021, 17, 191−200 Read Online

ACCESS | Metrics & More | Article Recommendations

ABSTRACT: In this work, we show the advantages of using the Coulomb hole plus screened exchange (COHSEX) approach in the calculation of potential energy surfaces (PES). In particular, we demonstrate that, unlike perturbative *GW* and partial self-consistent *GW* approaches, such as eigenvalue self-consistent *GW* and quasi-particle (QP) self-consistent *GW*, the COHSEX approach yields smooth PES without irregularities and discontinuities. Moreover, we show that the ground-state PES obtained from the Bethe−Salpeter equation (BSE), within the adiabatic connection fluctuation dissipation theorem, built with QP energies obtained from perturbative COHSEX on top of Hartree−Fock (BSE@COHSEX@HF) yield very accurate results for diatomic molecules close to their equilibrium distance. When self-consistent COHSEX QP energies and orbitals are used to build the BSE equation, the results become independent of the starting point. We show that self-consistency worsens the total energies but improves the equilibrium distances with respect to BSE@COHSEX@HF. This is mainly due to the changes in the screening inside the BSE.

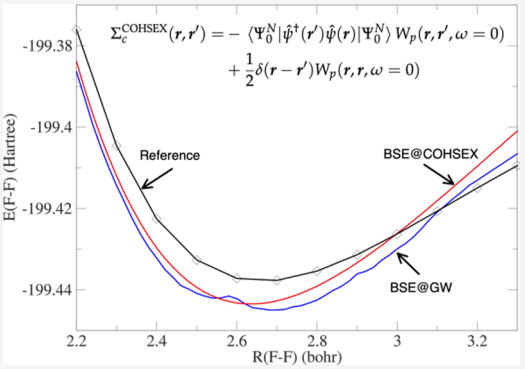

1. INTRODUCTION

In the last decade, the *GW* method[1−4] has become a standard tool in the quantum chemistry tool box. It has proved to be a powerful approach for the calculation of ionization energies, electron affinities, fundamental gaps, and so forth. However, because of the complexity of the *GW* self-energy, which is non-Hermitian and frequency-dependent, a fully self-consistent approach is nontrivial.[5−13] As a consequence, several approximate *GW* schemes have been devised. The most popular approaches are perturbative *GW*, also known as G_0W_0,[14−19] eigenvalue self-consistent *GW* (ev*GW*),[20−23] and quasi-particle (QP) self-consistent *GW* (qs*GW*).[24−28] Within G_0W_0, the *GW* self-energy is treated as a perturbation with respect to a zeroth-order Hamiltonian with a simpler self-energy, such as Hartree−Fock (HF), or a different Hamiltonian altogether, such as a Kohn−Sham Hamiltonian. The main drawback of G_0W_0 is its dependence on the choice of the starting point, that is, the zeroth-order Hamiltonian.[7,22,27−30] Within ev*GW*, the dependence on the starting point is reduced by updating the eigenvalues in a self-consistent field procedure. However, the orbitals remain those of the zeroth-order Hamiltonian. Finally, within qs*GW*, the *GW* self-energy is approximated in such a way that it is both Hermitian and frequency-independent. This allows for a simple self-consistent procedure for both eigenvalues and orbitals eliminating the influence of the starting point.

Although it is known that *GW* has some shortcomings, they have, until recently, mainly appeared in the strongly correlated regime.[31−39] However, in two recent articles,[40,41] we uncovered an important shortcoming of the G_0W_0, ev*GW*, and qs*GW* approaches that appears in the weakly correlated regime. All the three approaches suffer from unphysical irregularities and even discontinuities (ev*GW* and qs*GW*) in important physical quantities such as QP energies, neutral excitation energies, and correlation energies. We showed that the problem could be traced back to the existence of multiple close-lying solutions when the QP energy is close to a pole of the self-energy.[18,40−42] When the solution switches from one branch to another one, it yields an irregularity or discontinuity in the physical observable. The problem is more severe in ev*GW* and qs*GW* because, due to the self-consistency procedure, an irregularity in one QP energy is transferred to all QP energies through the self-consistent procedure.

This problem was again observed in the potential energy surfaces (PES) of diatomic molecules.[43] Accurate results were obtained for the ground-state total energies from the adiabatic-connection fluctuation−dissipation theorem (ACFDT)[44−54] applied to the Bethe−Salpeter equation (BSE) formalism.[55−58]

Received: August 27, 2020
Published: December 11, 2020

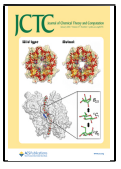

https://dx.doi.org/10.1021/acs.jctc.0c00896
J. Chem. Theory Comput. 2021, 17, 191−200

However, because the BSE calculations were performed on top of a G_0W_0 calculation, irregularities appeared in the energy curves because of the problem discussed above. As can be anticipated from our discussion above, switching to evGW or qsGW will not solve the problem. Below we will also explicitly show that discontinuities indeed appear in the PES when evGW or qsGW orbitals and energies are used to calculate the total energy. In view of the above, it is desirable to find an alternative approach to G_0W_0, evGW, and qsGW that does not suffer from this drawback and yields accurate total energies at an affordable computational cost.

In this work, we will consider the Coulomb hole plus screened exchange (COHSEX) self-energy, which was proposed a long time ago by Hedin,[1,20,59] both perturbatively, namely, on top of HF, and self-consistently (scCOHSEX).[60] Although the physics inside the COHSEX self-energy is very similar to that included in the GW self-energy, unlike the GW self-energy, it is Hermitian and frequency-independent. As a consequence, COHSEX calculations can be done self-consistently using standard numerical techniques (i.e., by simple diagonalization of a Fock-like operator). A self-consistent COHSEX calculation can also be used as a starting point for a G_0W_0 or evGW calculation.[60−66] Such an approach generally yields accurate energy gaps, but this would of course suffer from the same irregularities and discontinuities mentioned above. Thanks to its numerical efficiency COHSEX can be used to perform calculations on large systems.[67,68] The COHSEX approach can also be used to calculate ionic gradients.[69] Instead, the irregularities and discontinuities in G_0W_0, evGW, and qsGW could prevent a straightforward calculation of these quantities. Finally, we note that improvements of the COHSEX method have been proposed.[70]

The main goal of this work is twofold. We want to show that (i) physical observables, and in particular PES, obtained within the COHSEX approach do not suffer from irregularities and discontinuities and (ii) the PES and equilibrium geometries obtained from the BSE using perturbative COHSEX QP energies (i.e., BSE@COHSEX@HF) are comparable in accuracy to those obtained within BSE@G_0W_0@HF. We illustrate both points by calculating the PES and equilibrium distances (R_{eq}) of several diatomic molecules. Furthermore, we want to demonstrate that (iii) although the COHSEX and G_0W_0 energy gaps are quite different, the influence of this difference on the PES and equilibrium distances is small and (iv) for the diatomic molecules studied here, perturbative COHSEX, that is, BSE@COHSEX@HF, yields PES that are in better agreement with the reference values than self-consistent COHSEX, that is, BSE@scCOHSEX. Instead, the values of R_{eq} obtained within BSE@scCOHSEX are slightly improved with respect to BSE@COHSEX@HF when compared to the reference data.

The paper is organized as follows. In Section 2, we describe the theory behind the COHSEX approach and we also briefly discuss the theory of G_0W_0 and partially self-consistent GW methods. We report and discuss our results in Section 3. Finally, in Section 4, we draw the conclusions from our work.

2. THEORY

The key variable within many-body perturbation theory is the one-body Green's function G. In the absence of time-dependent fields and at zero temperature, it is defined as

$$G(\boldsymbol{r}, \boldsymbol{r}', \tau) = -i\Theta(\tau)\langle \Psi_0^N | \hat{\psi}(\boldsymbol{r}) e^{-i(\hat{H}^N - E_0^N)\tau} \hat{\psi}^\dagger(\boldsymbol{r}') | \Psi_0^N \rangle + i\Theta(-\tau)\langle \Psi_0^N | \hat{\psi}^\dagger(\boldsymbol{r}') e^{i(\hat{H}^N - E_0^N)\tau} \hat{\psi}(\boldsymbol{r}) | \Psi_0^N \rangle \quad (1)$$

where $\hat{H}^N$ is the Hamiltonian of the N-electron system, Ψ_0^N is its ground-state wave function, E_0^N is the ground-state energy, Θ is the Heaviside step function, while $\hat{\psi}^\dagger$ and $\hat{\psi}$ are creation and annihilation operators, respectively. In practice, the one-body Green's function can be obtained from the solution of the following Dyson equation

$$G(\boldsymbol{r}, \boldsymbol{r}', \tau) = G_{HF}(\boldsymbol{r}, \boldsymbol{r}', \tau) + \int\int d\boldsymbol{r}_1 d\boldsymbol{r}_2 \int\int d\tau_1 d\tau_2 G_{HF}(\boldsymbol{r}, \boldsymbol{r}_1, \tau - \tau_1) \Sigma_c(\boldsymbol{r}_1, \boldsymbol{r}_2, \tau_2) G(\boldsymbol{r}_2, \boldsymbol{r}', \tau_1 - \tau_2) \quad (2)$$

where G_{HF} is the one-body Green's function within the HF approximation and Σ_c is the correlation part of the self-energy, which has to be approximated in practical calculations.

2.1. COHSEX Self-Energy. In this section, we discuss the COHSEX self-energy and, in particular, its correlation part. We will compare it to the GW self-energy as the two self-energies are similar. The correlation parts of the GW and COHSEX self-energies are given by

$$\Sigma_c^{GW}(\boldsymbol{r}, \boldsymbol{r}', \tau) = iG(\boldsymbol{r}, \boldsymbol{r}', \tau) W_p(\boldsymbol{r}, \boldsymbol{r}', \tau + \eta) \quad (3a)$$

$$\Sigma_c^{COHSEX}(\boldsymbol{r}, \boldsymbol{r}', \tau) = iG(\boldsymbol{r}, \boldsymbol{r}', \tau) W_p(\boldsymbol{r}, \boldsymbol{r}', \omega = 0) \times [\delta(\tau + \eta) + \delta(\tau - \eta)]/2 \quad (3b)$$

where $W_p = W - v$ is the difference between the screened Coulomb interaction W and the bare Coulomb interaction v, δ is the Dirac delta function, and η is a positive infinitesimal that ensures the correct time ordering. The main difference between the two approximations is that the GW self-energy contains a dynamical (i.e., frequency-dependent) W_p, while the COHSEX self-energy has a static (i.e., frequency-independent) W_p. A Fourier transformation of eqs 3a and 3b yields the following two expressions

$$\Sigma_c^{GW}(\boldsymbol{r}, \boldsymbol{r}', \omega) = \frac{i}{2\pi} \int d\omega' e^{i\eta\omega'} G(\boldsymbol{r}, \boldsymbol{r}', \omega + \omega') W_p(\boldsymbol{r}, \boldsymbol{r}', \omega') \quad (4a)$$

$$\Sigma_c^{COHSEX}(\boldsymbol{r}, \boldsymbol{r}') = \frac{i}{2}[G(\boldsymbol{r}, \boldsymbol{r}', -\eta) + G(\boldsymbol{r}, \boldsymbol{r}', \eta)] W_p(\boldsymbol{r}, \boldsymbol{r}', \omega = 0) = \frac{1}{2}\langle \Psi_0^N | \hat{\psi}(\boldsymbol{r}) \hat{\psi}^\dagger(\boldsymbol{r}') - \hat{\psi}^\dagger(\boldsymbol{r}') \hat{\psi}(\boldsymbol{r}) | \Psi_0^N \rangle W_p(\boldsymbol{r}, \boldsymbol{r}', \omega = 0) \quad (4b)$$

and clearly shows that the COHSEX self-energy is static. We note that to better understand the screened exchange (SEX) and the Coulomb hole (COH) parts of the COHSEX self-energy, it is useful to rewrite eq 4b according to

$$\Sigma_c^{COHSEX}(\boldsymbol{r}, \boldsymbol{r}') = -\langle \Psi_0^N | \hat{\psi}^\dagger(\boldsymbol{r}') \hat{\psi}(\boldsymbol{r}) | \Psi_0^N \rangle W_p(\boldsymbol{r}, \boldsymbol{r}', \omega = 0) + \tfrac{1}{2}\delta(\boldsymbol{r} - \boldsymbol{r}') W_p(\boldsymbol{r}, \boldsymbol{r}, \omega = 0) \quad (5)$$

where we used the anti-commutator relation for the field operators, that is, $\hat{\psi}(\boldsymbol{r}')\hat{\psi}^\dagger(\boldsymbol{r}) + \hat{\psi}^\dagger(\boldsymbol{r}')\hat{\psi}(\boldsymbol{r}) = \delta(\boldsymbol{r} - \boldsymbol{r}')$. The first term on the right-hand side of eq 5 when combined with the HF exchange part of the self-energy, that is

$$\Sigma_x^{HF}(\boldsymbol{r}, \boldsymbol{r}') = -\langle \Psi_0^N | \hat{\psi}^\dagger(\boldsymbol{r}') \hat{\psi}(\boldsymbol{r}) | \Psi_0^N \rangle v(\boldsymbol{r}, \boldsymbol{r}') \quad (6)$$

yields the screened exchange self-energy. The second term on the right-hand side of eq 5 is the (static) Coulomb hole self-

https://dx.doi.org/10.1021/acs.jctc.0c00896
J. Chem. Theory Comput. 2021, 17, 191−200

energy because $W_p(\boldsymbol{r}, \boldsymbol{r}, \omega = 0)$ is the Coulomb potential at $\boldsymbol{r}$ because of the Coulomb hole created by an electron present at $\boldsymbol{r}$.

We can express W_p as

$$W_p(\boldsymbol{r}, \boldsymbol{r}', \omega) = \int\int \mathrm{d}\boldsymbol{r}_1 \mathrm{d}\boldsymbol{r}_2 v(\boldsymbol{r}, \boldsymbol{r}_1)\chi(\boldsymbol{r}_1, \boldsymbol{r}_2, \omega)v(\boldsymbol{r}_2, \boldsymbol{r}') \tag{7}$$

where the (reducible) polarizability χ can be written as

$$\chi(\boldsymbol{r}, \boldsymbol{r}', \omega) = \sum_m \left[\frac{\rho_m(\boldsymbol{r})\rho_m(\boldsymbol{r}')}{\omega - \Omega_m + i\eta} - \frac{\rho_m(\boldsymbol{r})\rho_m(\boldsymbol{r}')}{\omega + \Omega_m - i\eta}\right] \tag{8}$$

in which Ω_m is a neutral excitation energy and ρ_m is the corresponding transition density. The latter is defined as

$$\rho_m(\boldsymbol{r}) = \sum_i^{\mathrm{occ}} \sum_a^{\mathrm{virt}} (\mathbf{X} + \mathbf{Y})_m^{ia} \phi_i(\boldsymbol{r})\phi_a(\boldsymbol{r}) \tag{9}$$

where ϕ_p are either the (real-valued) HF spatial orbitals ϕ_p^{HF} (for a COHSEX@HF calculation) or the (real-valued) scCOHSEX spatial orbitals ϕ_p^{COHSEX}, that is, the eigenfunctions of the COHSEX Hamiltonian $\hat{H}^{\mathrm{COHSEX}} = \hat{H}^{\mathrm{HF}} + \hat{\Sigma}_c^{\mathrm{COHSEX}}$. In the following, the index m labels the single excitations; i and j are occupied orbitals; a and b are unoccupied orbitals; while p, q, r, and s indicate arbitrary orbitals.

The neutral excitation energies Ω_m and the transition amplitudes $(\mathbf{X} + \mathbf{Y})_m^{ia}$ are obtained from a random-phase approximation (RPA) calculation

$$\begin{pmatrix} \mathbf{A} & \mathbf{B} \\ -\mathbf{B} & -\mathbf{A} \end{pmatrix} \begin{pmatrix} \mathbf{X}_m \\ \mathbf{Y}_m \end{pmatrix} = \Omega_m \begin{pmatrix} \mathbf{X}_m \\ \mathbf{Y}_m \end{pmatrix} \tag{10}$$

where $(\mathbf{X}_m, \mathbf{Y}_m)^{\mathrm{T}}$ is the eigenvector that corresponds to Ω_m and

$$\mathrm{A}_{ia,jb} = \delta_{ij}\delta_{ab}(\epsilon_a - \epsilon_i) + 2(ia|jb) \tag{11a}$$

$$\mathrm{B}_{ia,jb} = 2(ia|bj) \tag{11b}$$

where ϵ_p are either the HF orbital energies ϵ_p^{HF} (for a COHSEX@HF calculation) or the scCOHSEX orbital energies $\epsilon_p^{\mathrm{COHSEX}}$ (i.e., the eigenvalues of $\hat{H}^{\mathrm{COHSEX}}$), and $(pq|rs)$ are the bare two-electron integrals defined as

$$(pq|rs) = \iint \mathrm{d}\boldsymbol{r}\mathrm{d}\boldsymbol{r}' \phi_p(\boldsymbol{r})\phi_q(\boldsymbol{r})v(\boldsymbol{r}, \boldsymbol{r}')\phi_r(\boldsymbol{r}')\phi_s(\boldsymbol{r}') \tag{12}$$

While the GW self-energy is non-Hermitian and frequency-dependent, the COHSEX self-energy is both static and Hermitian as can be verified from the expression one obtains by inserting eq 8 into 4b (with W_p given by 7)

$$\Sigma_c^{\mathrm{COHSEX}}(\boldsymbol{r}, \boldsymbol{r}') = [\langle \Psi_0^N|\hat{\psi}^\dagger(\boldsymbol{r}')\hat{\psi}(\boldsymbol{r})|\Psi_0^N\rangle - \langle \Psi_0^N|\hat{\psi}(\boldsymbol{r})\hat{\psi}^\dagger(\boldsymbol{r}')|\Psi_0^N\rangle] \times \iint \mathrm{d}\boldsymbol{r}_1\mathrm{d}\boldsymbol{r}_2 v(\boldsymbol{r}, \boldsymbol{r}_1)\sum_m \frac{\rho_m(\boldsymbol{r}_1)\rho_m(\boldsymbol{r}_2)}{\Omega_m} v(\boldsymbol{r}_2, \boldsymbol{r}') \tag{13}$$

Moreover, it is important to note that the COHSEX self-energy has no poles. More precisely, its denominator never vanishes because Ω_m are real and positive for finite systems. Owing to the Hermiticity and frequency independence of the COHSEX self-energy, Ψ_0^N can be represented by a single Slater determinant. Following the Slater−Condon rules, the matrix elements in the above equation can then be rewritten as sums of products of orbitals. We obtain

$$\Sigma_c^{\mathrm{COHSEX}}(\boldsymbol{r}, \boldsymbol{r}') = 2\left[\sum_i^{\mathrm{occ}} \phi_i(\boldsymbol{r})\phi_i(\boldsymbol{r}') - \sum_a^{\mathrm{virt}} \phi_a(\boldsymbol{r})\phi_a(\boldsymbol{r}')\right] \times \iint \mathrm{d}\boldsymbol{r}_1\mathrm{d}\boldsymbol{r}_2 v(\boldsymbol{r}, \boldsymbol{r}_1)\sum_m \frac{\rho_m(\boldsymbol{r}_1)\rho_m(\boldsymbol{r}_2)}{\Omega_m} v(\boldsymbol{r}_2, \boldsymbol{r}') \tag{14}$$

The matrix element $\Sigma_{c,pq}^{\mathrm{COHSEX}} = \langle \phi_p|\Sigma_c^{\mathrm{COHSEX}}|\phi_q\rangle$ can now be written as

$$\Sigma_{c,pq}^{\mathrm{COHSEX}} = 2\sum_m \left[\sum_i^{\mathrm{occ}} \frac{[pi|m][qi|m]}{\Omega_m} - \sum_a^{\mathrm{virt}} \frac{[pa|m][qa|m]}{\Omega_m}\right] \tag{15}$$

where the screened two-electron integrals are defined as

$$[pq|m] = \sum_{ia} (pq|ia)(\mathbf{X} + \mathbf{Y})_m^{ia} \tag{16}$$

When COHSEX is performed using first-order perturbation theory with respect to HF, the perturbation is given by $\hat{H}^{\mathrm{COHSEX}} - \hat{H}^{\mathrm{HF}} = \hat{\Sigma}_c^{\mathrm{COHSEX}}$. The perturbative COHSEX orbital energies can thus be obtained from

$$\epsilon_p^{\mathrm{COHSEX}} = \epsilon_p^{\mathrm{HF}} + \Sigma_{c,pp}^{\mathrm{COHSEX}} \tag{17}$$

Instead, within scCOHSEX, both the eigenvalues and eigenfunctions of the COHSEX Hamiltonian have to be calculated repeatedly until a self-consistent result is obtained.

2.2. G_0W_0. Given the difficulty of evaluating the GW self-energy mentioned above, one often uses a perturbative approach called G_0W_0 in which the self-energy is calculated perturbatively with respect to a simpler zeroth-order Hamiltonian, such as a self-energy for which a self-consistent solution is more easily obtained. In this work, we will use the HF Green's function as our zeroth-order Green's function. Its spectral representation is given by

$$G_{\mathrm{HF}}(\boldsymbol{r}, \boldsymbol{r}', \omega) = \sum_p \frac{\phi_p^{\mathrm{HF}}(\boldsymbol{r})\phi_p^{\mathrm{HF}}(\boldsymbol{r}')}{\omega - \epsilon_p^{\mathrm{HF}} - i\eta\mathrm{sign}(\mu - \epsilon_p^{\mathrm{HF}})} \tag{18}$$

with μ being the chemical potential. Within the G_0W_0 approximation, the frequency integral in eq 4a can be performed analytically and one obtains the following matrix elements of the G_0W_0 self-energy

$$\Sigma_{c,pq}^{G_0W_0}(\omega) = 2\sum_m \left[\sum_i^{\mathrm{occ}} \frac{[pi|m]^{\mathrm{HF}}[qi|m]^{\mathrm{HF}}}{\omega - \epsilon_i^{\mathrm{HF}} + \Omega_m^{\mathrm{HF}} - i\eta} + \sum_a^{\mathrm{virt}} \frac{[pa|m]^{\mathrm{HF}}[qa|m]^{\mathrm{HF}}}{\omega - \epsilon_a^{\mathrm{HF}} - \Omega_m^{\mathrm{HF}} + i\eta}\right] \tag{19}$$

where the superscript in Ω_m^{HF} and $[pq|m]^{\mathrm{HF}}$ indicates that these quantities are obtained from HF eigenvalues and orbitals. Contrary to the COHSEX self-energy, the above self-energy is dynamical and has poles. The QP energies can then be obtained from the poles of G obtained by solving the Dyson eq 2 (in frequency space) with the above self-energy. This yields the so-called QP equation

$$\omega = \epsilon_p^{\mathrm{HF}} + \mathrm{Re}\left[\Sigma_{c,pp}^{G_0W_0}(\omega)\right] \tag{20}$$

Because of the frequency dependence of the self-energy, the G_0W_0 QP equation has, in general, multiple solutions $\epsilon_{p,s}^{G_0W_0}$.

https://dx.doi.org/10.1021/acs.jctc.0c00896
J. Chem. Theory Comput. 2021, 17, 191−200

The solution $\epsilon_p^{G_0W_0} \equiv \epsilon_{p,s=0}^{G_0W_0}$ with the largest spectral weight $Z_p(\epsilon_{p,s=0}^{G_0W_0})$ with

$$Z_p(\omega) = \left[1 - \frac{\mathrm{Re}\left[\Sigma_{c,pp}^{G_0W_0}(\omega)\right]}{\partial\omega}\right]^{-1} \tag{21}$$

is called the QP solution (or simply QP), while the other solutions ($s > 0$) are called satellites and share the rest of the spectral weight. In practice, the QP equation is often simplified by Taylor expanding the self-energy to first order around ϵ_p^{HF}. The result is the so-called linearized QP equation given by

$$\epsilon_p^{G_0W_0} = \epsilon_p^{\mathrm{HF}} + Z_p(\epsilon_p^{\mathrm{HF}})\mathrm{Re}\left[\Sigma_{c,pp}^{G_0W_0}(\epsilon_p^{\mathrm{HF}})\right] \tag{22}$$

When the self-energy has poles close to a solution of the QP equation, the above linearization is not justified. Moreover, it leads to irregularities in physical observables such as PES. This can be understood as follows.

Although the self-energy in the linearized QP equation is independent of the frequency, its denominator could still vanish. This happens when $\epsilon_p^{\mathrm{HF}} = \epsilon_i^{\mathrm{HF}} - \Omega_m^{\mathrm{HF}}$ or when $\epsilon_p^{\mathrm{HF}} = \epsilon_a^{\mathrm{HF}} + \Omega_m^{\mathrm{HF}}$. When calculating a single QP for a single configuration of an atom or a molecule, it is not very probable that such an event occurs. However, when a large number of QPs and/or configurations is considered, for example, when calculating a PES, it becomes inevitable. As an example, let us consider the simplest PES, namely, the variation of the total energy of a diatomic molecule as a function of the interatomic distance R. In such a case, ϵ_p^{HF} and Ω_m^{HF} could be considered functions of R and the conditions that the self-energy has a vanishing denominator can be written as

$$\epsilon_p^{\mathrm{HF}}(R) = \epsilon_i^{\mathrm{HF}}(R) - \Omega_m^{\mathrm{HF}}(R) \tag{23a}$$

$$\epsilon_p^{\mathrm{HF}}(R) = \epsilon_a^{\mathrm{HF}}(R) + \Omega_m^{\mathrm{HF}}(R) \tag{23b}$$

Therefore, $\Sigma_{c,pp}^{G_0W_0}[\epsilon_p^{\mathrm{HF}}(R)]$ can be considered an implicit function of R that has poles. From the above conditions, it is clear that in a region equal to $2\Omega_0^{\mathrm{HF}}(R) + \epsilon_{\mathrm{LUMO}}^{\mathrm{HF}}(R) - \epsilon_{\mathrm{HOMO}}^{\mathrm{HF}}(R)$ around the Fermi level, no poles can occur, where Ω_0^{HF} is the smallest neutral excitation energy and $\epsilon_{\mathrm{LUMO}}^{\mathrm{HF}}$ and $\epsilon_{\mathrm{HOMO}}^{\mathrm{HF}}$ are the HF energies of the lowest unoccupied molecular orbital (LUMO) and the highest occupied molecular orbital (HOMO), respectively. However, because, in general, the variation with respect to R of the left- and right-hand sides of eqs 23a and 23b is different, it is unavoidable that outside of this range, one of the two above conditions is met for some values $R = R_p$. In the vicinity of these R_p values, the self-energy [see eq 19] and its corresponding renormalization factor Z_p [see eq 21] vary rapidly, leading to irregularities in the QP energies and, hence, in the PES. We note that satisfaction of either eqs 23a or 23b will ensure an irregularity and that they can never be met simultaneously.

2.3. Partially Self-Consistent *GW*. The main drawback of the G_0W_0 approach is its dependence on the starting point, that is, the orbitals and energies of the zeroth-order Hamiltonian. Because, as mentioned above, from a numerical point of view, fully self-consistent *GW* is nontrivial, the so-called partial self-consistent *GW* methods have been developed to reduce or eliminate the starting point dependence. Within ev*GW*, one only updates the eigenvalues in the self-energy, while in qs*GW*, one symmetrizes the G_0W_0 self-energy according to

$$\Sigma_{c,pq}^{\mathrm{qs}GW} = \frac{1}{2}\mathrm{Re}\left[\Sigma_{c,pq}^{G_0W_0}(\epsilon_p^{\mathrm{qs}GW}) + \Sigma_{c,pq}^{G_0W_0}(\epsilon_q^{\mathrm{qs}GW})\right] \tag{24}$$

The above self-energy is frequency-independent and Hermitian and is, hence, suitable for a standard self-consistent procedure. Therefore, in this partially self-consistent scheme, both the eigenvalues and orbitals are updated.

However, the ev*GW* and qs*GW* approaches suffer from the same problem as G_0W_0 because the self-energies have poles when considered as (implicit) functions of the geometry. In fact, the problem is even more severe because, due to the self-consistent procedure, an irregularity in one QP energy is transferred to all the other QP energies. As a consequence, in some regions of the geometry space, there is more than one branch of solutions and discontinuities appear when a solution switches from one branch to another.

To be more precise, let us consider a diatomic molecule. For certain internuclear distances R_d, two solutions of the QP equation can have equal weight but not equal energies. Just before this point R_d, one of the two solutions will be picked up in the self-consistent procedure because it has a slightly larger weight than the other solution. Instead, just after R_d, the roles are reversed and the other solution will be picked up because it is now the one with the slightly larger weight. Because the two solutions have different energies, there is a sudden jump of the QP energy at R_d causing a discontinuity. This scenario occurs whenever a solution of the QP equation lies close to a pole of the self-energy.[40,41] It can happen for any state, occupied or virtual, except those close to the Fermi level because, as mentioned before, the self-energy has no poles there. More details and analysis of the origin of irregularities and discontinuities in *GW* approaches can be found in refs.[40,41]

2.4. Correlation Energy. We calculate the correlation energies at the BSE level using an approach based on the ACFDT.[44−46] We note that the ACFDT formalism is formally derived for a local potential, while here the potential, that is, the self-energy, is nonlocal. We strictly follow the ACFDT procedure described in ref 43 and the details can be found there. For the sake of completeness, we briefly discuss some details of the calculation of the BSE total energy. The main difference with ref 43 is that the QP energies and orbitals appearing in the equations below are those pertaining to the COHSEX self-energy instead of the G_0W_0 self-energy. Finally, we note that the approach described below is compatible only with a QP calculation but not fully self-consistent *GW* because it requires orbitals and orbital energies as input.

Within the ACFDT formalism, the BSE correlation energy can be written as an integral over the coupling constant λ, which adiabatically connects the noninteracting system ($\lambda = 0$) with the fully interacting system ($\lambda = 1$) according to[43,50−54]

$$E_c^{\mathrm{BSE}} = \frac{1}{2}\int_0^1 \mathrm{Tr}(\mathbf{K}\mathbf{P}^\lambda)\mathrm{d}\lambda \tag{25}$$

where the polarizability matrix $\mathbf{P}^\lambda$ is given by

$$\mathbf{P}^\lambda = \begin{pmatrix} \mathbf{Y}^\lambda(\mathbf{Y}^\lambda)^{\mathrm{T}} & \mathbf{Y}^\lambda(\mathbf{X}^\lambda)^{\mathrm{T}} \\ \mathbf{X}^\lambda(\mathbf{Y}^\lambda)^{\mathrm{T}} & \mathbf{X}^\lambda(\mathbf{X}^\lambda)^{\mathrm{T}} \end{pmatrix} - \begin{pmatrix} 0 & 0 \\ 0 & 1 \end{pmatrix} \tag{26}$$

with $\mathbf{X}^\lambda$ and $\mathbf{Y}^\lambda$ solutions of

$$\begin{pmatrix} \mathbf{A}^{\lambda,\mathrm{BSE}} & \mathbf{B}^{\lambda,\mathrm{BSE}} \\ -\mathbf{B}^{\lambda,\mathrm{BSE}} & -\mathbf{A}^{\lambda,\mathrm{BSE}} \end{pmatrix} \begin{pmatrix} \mathbf{X}_m^\lambda \\ \mathbf{Y}_m^\lambda \end{pmatrix} = \Omega_m^\lambda \begin{pmatrix} \mathbf{X}_m^\lambda \\ \mathbf{Y}_m^\lambda \end{pmatrix} \tag{27}$$

https://dx.doi.org/10.1021/acs.jctc.0c00896
J. Chem. Theory Comput. 2021, 17, 191−200

where

$$A^{\lambda,\mathrm{BSE}}_{ia,jb} = \delta_{ij}\delta_{ab}(\epsilon_a - \epsilon_i) + \lambda[2(ialjb) - W^{\lambda}_{ij,ab}] \quad (28)$$

$$B^{\lambda,\mathrm{BSE}}_{ia,jb} = \lambda[2(ialbj) - W^{\lambda}_{ib,aj}] \quad (29)$$

with

$$W^{\lambda}_{pq,rs} = \iint \mathrm{d}\boldsymbol{r}\mathrm{d}\boldsymbol{r}'\phi_p(\boldsymbol{r})\phi_q(\boldsymbol{r})W^{\lambda}(\boldsymbol{r}, \boldsymbol{r}', \omega = 0)\phi_r(\boldsymbol{r}')\phi_s(\boldsymbol{r}') \quad (30)$$

Finally, the interaction kernel $\mathbf{K}$ is given by

$$\mathbf{K} = \begin{pmatrix} \tilde{\mathbf{A}}^{\mathrm{BSE}} & \mathbf{B}^{\lambda=1,\mathrm{BSE}} \\ \mathbf{B}^{\lambda=1,\mathrm{BSE}} & \tilde{\mathbf{A}}^{\mathrm{BSE}} \end{pmatrix} \quad (31)$$

with $\tilde{A}^{\mathrm{BSE}}_{ia,jb} = 2(ialbj)$. We note that eq 25 is referred to as "extended Bethe−Salpeter (XBS)" in ref 52. An important point to make here is that, in contrast to Kohn−Sham density functional theory where the electron density is fixed along the adiabatic path,[44,45] the density is not maintained in the present BSE formalism as the coupling constant varies. Therefore, an additional contribution to eq 25 originating from the variation of the Green's function along the adiabatic connection path should be, in principle, added.[71] However, as it is commonly done,[47,48,52,72] we shall neglect it in the present study.

The BSE total energy E^{BSE} of the system can then be written as

$$E^{\mathrm{BSE}} = E^{\mathrm{nuc}} + E^{\mathrm{HF}} + E_c^{\mathrm{BSE}} \quad (32)$$

where E^{nuc} and E^{HF} are the nuclear energy and the HF energy, respectively. We note that for a BSE@scCOHSEX calculation, E^{HF} is calculated with the scCOHSEX orbitals.

3. RESULTS

All systems under investigation have a closed-shell singlet ground state. Hence, the restricted HF formalism has been systematically employed in the present study. The infinitesimal η is set to zero for all calculations. The numerical integration required to compute the correlation energy along the adiabatic path (see eq 25) is performed with a 21-point Gauss−Legendre quadrature. All the calculations have been performed with the software QuAcK,[73] freely available on GitHub. QuAcK uses Gaussian-type orbitals and its implementation closely follows that of MOLGW.[74] In particular, the frequency integral in the G_0W_0 self-energy is done exactly, that is, we solve eq 10 and use the neutral excitation energies in eq 19. The threshold for the convergence of the QP energies was set to 10^{-6} Ha and 10^{-5} Ha in the HF and scCOHSEX calculations, respectively. We have used the DIIS technique to accelerate convergence.[75,76] As one-electron basis sets, we employ the Dunning family (cc-pVXZ) defined with Cartesian Gaussian functions. Finally, we note that we diagonalize eq 10, which is a $(OV) \times (OV)$ matrix (where O and V are the number of occupied and virtual orbitals). Because a complete diagonalization scales as N^3, with N being the number of electrons, for a matrix of size $N \times N$, computing the screening in such a way scales as $(OV)^3$, that is, N^6. Several techniques exist to improve the scaling of the calculation of the screening.[77−81]

3.1. Irregularities and Discontinuities in G_0W_0, ev*GW*, and qs*GW*. We have previously described in detail the problem of irregularities and discontinuities in physical observables obtained from G_0W_0 and partially self-consistent *GW* approaches.[40,41] Here, we want to remind the reader that these problems are also present in total energy calculations and we want to show that, instead, there are no such problems in the COHSEX method. In Figure 1, we report the BSE total energy of the LiF molecule as a function of the interatomic distance in the vicinity of its equilibrium distance. The BSE correlation energy is calculated on top of G_0W_0@HF, COHSEX@HF, ev*GW*@HF, qs*GW*, and scCOHSEX. We used a relatively small basis set, namely, Dunning's cc-pVDZ basis, because for larger basis sets, the qs*GW* approach does not yield converged results for many values of R. This, however, does not change the conclusions of this section. We note that within qs*GW*, the entire set of energies and orbitals is updated at each iteration. We see that all four results are within a range of about 10 mHartree. However, the PES obtained from BSE@G_0W_0@HF shows irregularities, while the PES obtained from BSE@ev*GW*@HF and BSE@qs*GW* shows discontinuities. In fact, the different branches of solutions can clearly be seen, especially around 3.4 bohr. Instead, the BSE total energies obtained on top of a COHSEX calculation, that is, BSE@COHSEX@HF and BSE@scCOHSEX, yield a PES that is a smooth function of the interatomic distance.

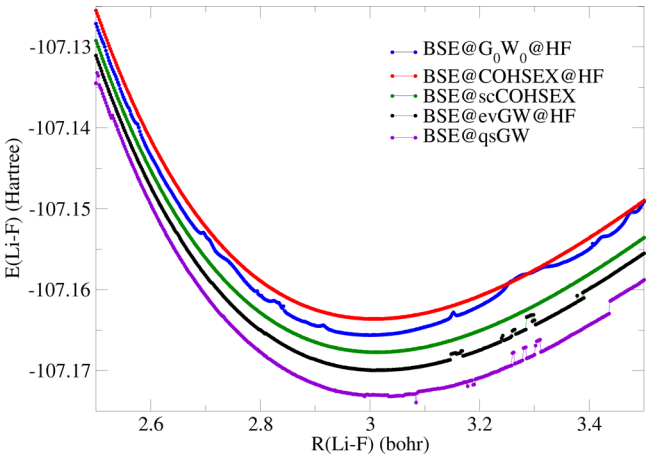

Figure 1. BSE total energy of the LiF molecule in the cc-pVDZ basis as a function of the internuclear distance. The calculations were done at intervals of 0.002 bohr.

Finally, we note that including self-consistency in COHSEX and *GW* tends to lower the total energies and that including self-consistency for both QP energies and orbitals lowers the total energy more than just including self-consistency for the QP energies. Moreover, the effect of self-consistency on the total energies in COHSEX, going from COHSEX@HF to scCOHSEX, is roughly identical to the effect on *GW*, going from G_0W_0@HF to ev*GW*@HF.

3.2. Ground-State PES. In Figures 2−9, we report the BSE total energies on top of COHSEX@HF, G_0W_0@HF, and scCOHSEX as a function of the interatomic distance around the equilibrium distance for the following diatomic molecules: H_2, LiH, LiF, HCl, N_2, CO, BF, and F_2, respectively. They are the same molecules that were studied in ref 43. We also use the same basis set, namely, Dunning's cc-pVQZ. For comparison, we also report the PES obtained with coupled-cluster (CC) methods of increasing accuracy: CC2,[82] CCSD,[83] and CC3.[84] At the equilibrium distance, the CC3 approach has been shown to yield total energies that are very close to those

https://dx.doi.org/10.1021/acs.jctc.0c00896
J. Chem. Theory Comput. 2021, 17, 191−200

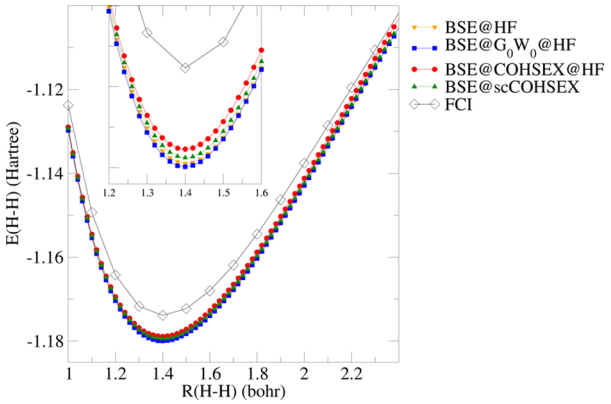

Figure 2. Total energy of the H_2 molecule in the cc-pVQZ basis as a function of the internuclear distance.

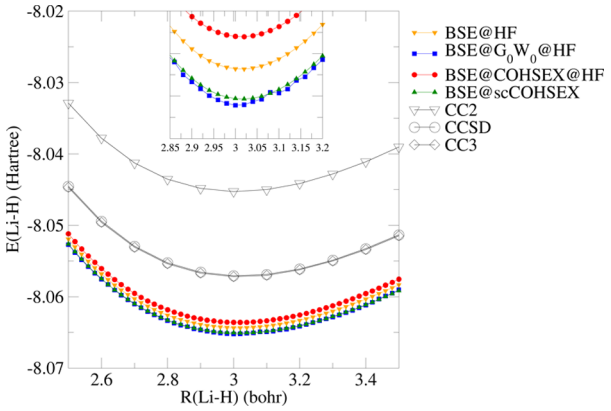

Figure 3. Total energy of the LiH molecule in the cc-pVQZ basis as a function of the internuclear distance.

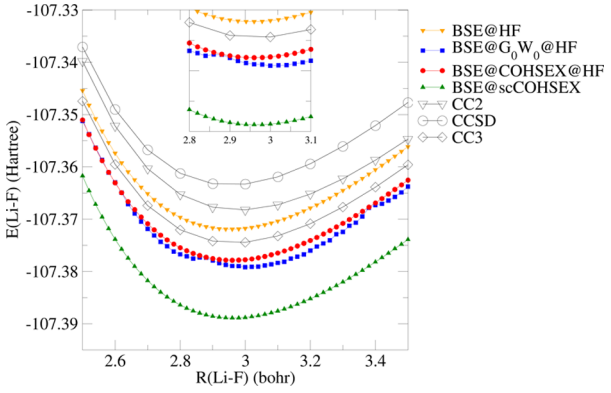

Figure 4. Total energy of the LiF molecule in the cc-pVQZ basis as a function of the internuclear distance.

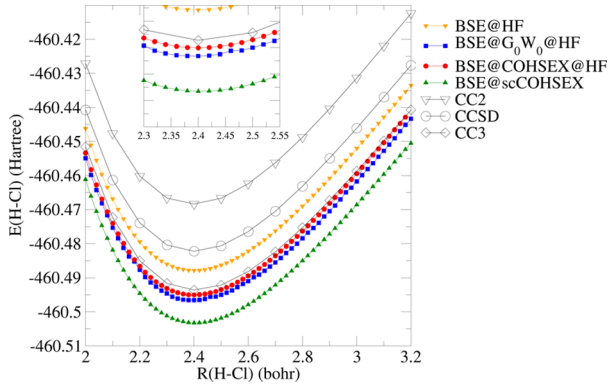

Figure 5. Total energy of the HCl molecule in the cc-pVQZ basis as a function of the internuclear distance.

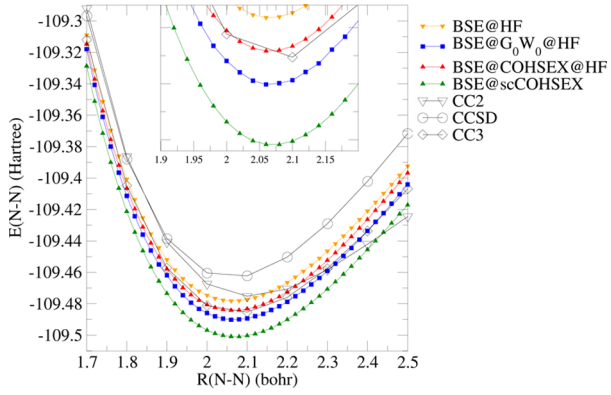

Figure 6. Total energy of the N_2 molecule in the cc-pVQZ basis as a function of the internuclear distance.

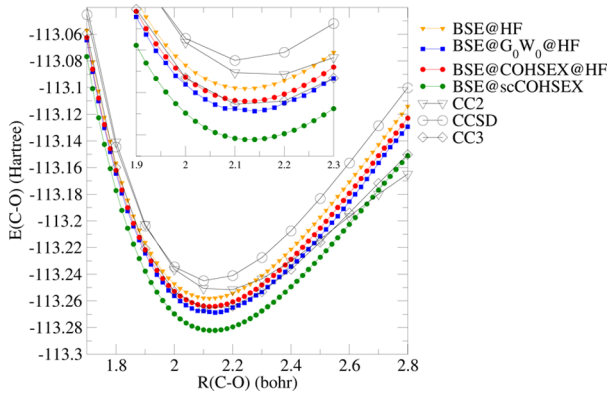

Figure 7. Total energy of the CO molecule in the cc-pVQZ basis as a function of the internuclear distance.

obtained with higher-order CC approaches, such as CCSDT and CCSDT(Q).[43] Therefore, we can consider it to be the reference method. We also compare to the PES obtained within BSE@HF in which the BSE is solved using HF orbital energies.

In the only case for which we have an exact result (for the given basis set), namely, the H_2 PES obtained from full configuration interaction (FCI), all BSE total energies are roughly the same. We also note that no irregularities are visible in the BSE@G_0W_0@HF curve. In the case of LiH, the second smallest molecule in the set, an irregularity appears in the BSE@G_0W_0@HF curve around 3.08 bohr. We also observe that the smooth BSE@COHSEX@HF total−energy curves are the closest to the reference CC3 values, while BSE@scCOHSEX and BSE@G_0W_0@HF yield almost identical energies. For the LiF molecule, there are large irregularities in the PES obtained within BSE@G_0W_0@HF around 2.9 bohr, which impedes a straightforward determination of the equilibrium distance (see below). Another large irregularity appears around 3.4 bohr. Again, the smooth BSE@COHSEX@HF curve is closer to that obtained within CC3 than the BSE@G_0W_0@HF curve, although the differences are small. Similar to the LiF results obtained above for the small cc-pVDZ basis, we observe again that including self-consistency in the COHSEX

https://dx.doi.org/10.1021/acs.jctc.0c00896
J. Chem. Theory Comput. 2021, 17, 191−200

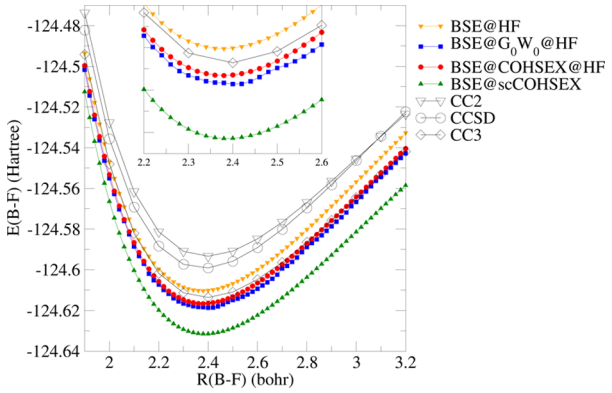

Figure 8. Total energy of the BF molecule in the cc-pVQZ basis as a function of the internuclear distance.

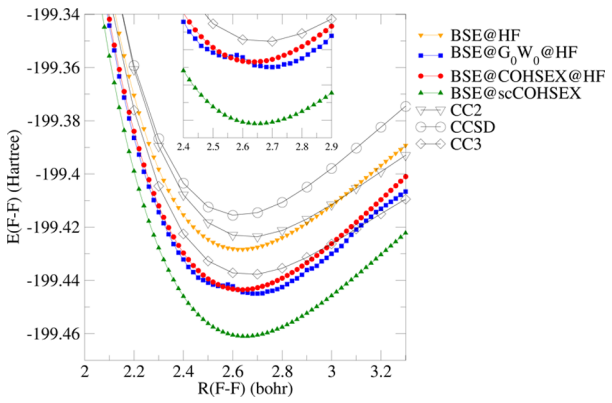

Figure 9. Total energy of the F_2 molecule in the cc-pVQZ basis as a function of the internuclear distance.

calculation lowers the total energy, thereby worsening the agreement with the CC reference data. Finally, we note that for LiF, the BSE@HF total energies are slightly closer to the reference CC3 results than those obtained within BSE@COHSEX@HF. However, as we will see in the following, the PES obtained within BSE@COHSEX@HF results are, in general, better than those obtained within BSE@HF.

The PES of all diatomic molecules, except the smallest two (H_2 and LiH), show similar trends as LiF, that is, small differences between the BSE@COHSEX@HF and BSE@G_0W_0@HF total energies and a relatively large difference with respect to the BSE@scCOHSEX total energies. Therefore, we conclude that the self-consistency has a much larger influence on the PES than the difference in the COHSEX and *GW* self-energies.

The PES of the HCl, N_2, CO, and BF molecules obtained within BSE@G_0W_0@HF all exhibit small irregularities, while those in F_2 are very large, preventing a simple determination of the F_2 equilibrium distance (see below). Again, BSE@COHSEX@HF is in excellent agreement with the CC3 results and even slightly better than those obtained within BSE@G_0W_0@HF, and, most importantly, the PES obtained within BSE@COHSEX@HF (and BSE@scCOHSEX) are devoid of irregularities and discontinuities.

In Table 1, we report the equilibrium distances obtained within the various BSE approaches and we compare them to the CC3 reference values and to the experimental values. As mentioned above, the irregularities in the PES can prevent a straightforward determination of the equilibrium distance. Therefore, following ref 43, for LiF and F_2, a Morse potential was used to fit the total energies in order to estimate the equilibrium distance. Although the total energies obtained within BSE@scCOHSEX were not as accurate as those obtained using perturbative QP energies, adding self-consistency to the COHSEX approach improves the equilibrium distances. In summary, while BSE@COHSEX@HF yields the smallest errors for the total energies, BSE@scCOHSEX yields the smallest errors for the equilibrium distances.

Finally, in order to estimate the influence of the QP energies on the BSE total energies, we report the ionization potentials (IPs) and the HOMO−LUMO gaps at the equilibrium distance corresponding to each level of theory for the various BSE approaches in Tables 2 and 3, respectively, and we compare to experimental data (when available). For the IPs, we also report the CCSD(T)/def2TZVPP data of ref 86, which are in good agreement with the experimental values with the exception of H_2. Comparing the differences in the IP with the differences in the PES, there does not emerge a clear link between the two. Although the IP obtained within COHSEX@HF and G_0W_0@HF show large differences, the differences between the corresponding BSE total energies are small. Instead, the differences in the IP between scCOHSEX and COHSEX@HF are small (except for N_2), but the differences in the corresponding total energies are large. Similarly, the differences in the IP between HF and G_0W_0@HF are often small, but the differences in the corresponding total energies are large. An equivalent analysis holds for the HOMO−LUMO gaps. Moreover, despite the fact that COHSEX@HF yields IP and HOMO−LUMO gaps significantly worse than those obtained within G_0W_0@HF when compared to the experimental values, the corresponding BSE total energies are very similar (except for the irregularities in G_0W_0@HF@BSE). Therefore, at least for the small molecules discussed here, the BSE total energies obtained within ACFDT seem to be robust with respect to the screening used in the calculation of the underlying QP energies. Instead, the total energies are sensitive

Table 1. Equilibrium Distances (in bohr) Obtained in the cc-pVQZ Basis Set[a]

	H_2	LiH	LiF	HCl	N_2	CO	BF	F_2
CC3	1.402	3.019	2.963	2.403	2.075	2.136	2.390	2.663
BSE@HF	1.402	3.014	2.954	2.400	2.065	2.120	2.378	2.631
BSE@G_0W_0@HF	1.399	3.017	(2.973)	2.400	2.065	2.134	2.385	(2.638)
BSE@COHSEX@HF	1.399	3.014	2.961	2.400	2.066	2.125	2.379	2.635
BSE@scCOHSEX	1.401	3.016	2.963	2.404	2.070	2.130	2.387	2.650
experiment	1.401	3.015	2.948	2.409	2.074	2.132	2.386	2.668

[a]The experimental values are extracted from ref 85. The results in brackets for LiF and F_2 were obtained by fitting the total energies to a Morse potential because the irregularities in the PES precluded a direct evaluation.

https://dx.doi.org/10.1021/acs.jctc.0c00896
J. Chem. Theory Comput. 2021, 17, 191−200

Table 2. IPs (in eV) at the Equilibrium Distance Obtained in the cc-pVQZ Basis Set Except for the CCSD(T) Values from ref 86, which Have Been Obtained in the def2-TZVPP Basis[a]

	H_2	LiH	LiF	HCl	N_2	CO	BF	F_2
HF	16.17	7.99	12.94	12.98	16.76	15.07	11.01	18.02
G_0W_0@HF	16.57	8.26	11.59	12.98	17.33	14.91	11.41	16.50
COHSEX@HF	18.05	9.52	13.82	14.49	19.48	16.69	12.86	18.88
scCOHSEX	17.83	9.21	13.12	14.02	17.52	15.79	12.45	18.00
CCSD(T)	16.40	7.96	11.32	12.59	15.57	14.21	11.09	15.71
experiment	15.43	7.90	11.30	12.79	15.58	14.01	11.00	15.70

[a]The experimental values are extracted from ref 18.

Table 3. HOMO−LUMO Gaps (in eV) at the Equilibrium Distance Obtained in the cc-pVQZ Basis Set[a]

	H_2	LiH	LiF	HCl	N_2	CO	BF	F_2
HF	20.08	8.08	12.72	15.76	20.95	18.55	13.15	20.80
G_0W_0@HF	20.24	8.04	11.31	15.20	20.24	17.33	12.90	17.32
COHSEX@HF	21.59	9.27	13.54	16.45	21.38	18.44	13.97	18.14
scCOHSEX	21.57	8.99	12.84	16.07	20.09	17.93	13.73	17.81
experiment		8.24						16.94

[a]The experimental values are extracted from ref 51.

to the screening that enters the BSE. Within BSE@COHSEX@HF and BSE@G_0W_0@HF, this quantity is identical because in both cases, it is calculated from the HF orbitals and energies. However, when one includes self-consistency, the screening changes and it has a significant influence on the total energy. We can therefore conclude that the screened Coulomb potential is the key quantity in the calculation of correlation energies within the ACFDT@BSE formalism and ultimately dictates the accuracy of the total energy. Nevertheless, when screening is completely neglected in the calculation of the QP energies, for example, in BSE@HF, this also has a significant influence on the results.

Finally, we note that, although BSE@COHSEX@HF gives the best PES and BSE@scCOHSEX the best equilibrium distances, the COHSEX@HF and scCOHSEX IPs and HOMO−LUMO gaps are not very good. Therefore, it would be desirable to find an improved static self-energy, which could give both smooth PES and good QP energies.

4. CONCLUSIONS

We have demonstrated that COHSEX is a promising approach to obtain QP energies for the calculation of PES. Contrary to G_0W_0 and partially self-consistent *GW* approaches, COHSEX yields results without irregularities and discontinuities. We have illustrated this feature by calculating the ground-state PES of diatomic molecules. Moreover, we have shown that BSE total energies of diatomic molecules using COHSEX QP energies obtained perturbatively on top of a HF calculation are in good agreement with accurate CC results. Finally, we showed that including self-consistency in the COHSEX approach for both QP energies and orbitals, in order to make the results independent of the starting point, worsens the total energies but improves the equilibrium distances. This is mainly due to variations in the screening *W* that enters the BSE.

AUTHOR INFORMATION

Corresponding Author

J. Arjan Berger − *Laboratoire de Chimie et Physique Quantiques, Université de Toulouse, CNRS, UPS, and European Theoretical Spectroscopy Facility (ETSF), Toulouse 31062, France;* orcid.org/0000-0002-4823-520X; Email: arjan.berger@irsamc.ups-tlse.fr

Authors

Pierre-François Loos − *Laboratoire de Chimie et Physique Quantiques, Université de Toulouse, CNRS, UPS, Toulouse 31062, France;* orcid.org/0000-0003-0598-7425

Pina Romaniello − *Laboratoire de Physique Théorique, Université de Toulouse, CNRS, UPS, and European Theoretical Spectroscopy Facility (ETSF), Toulouse 31062, France;* orcid.org/0000-0001-8300-8320

Complete contact information is available at: https://pubs.acs.org/10.1021/acs.jctc.0c00896

Notes

The authors declare no competing financial interest.

ACKNOWLEDGMENTS

J.A.B. and P.R. thank the French Agence Nationale de la Recherche (ANR) for financial support (grant agreements ANR-18-CE30-0025 and ANR-19-CE30-0011). PFL thanks the European Research Council (ERC) under the European Union's Horizon 2020 research and innovation programme (grant agreement no. 863481) for financial support. This study has also been partially supported through the EUR grant NanoX no ANR-17-EURE-0009 in the framework of the "Programme des Investissements d'Avenir." J.A.B. thanks Anthony Scemama for technical support.

REFERENCES

(1) Hedin, L. New Method for Calculating the One-Particle Green's Function with Application to the Electron-Gas Problem. *Phys. Rev.* **1965**, *139*, A796.

(2) Aryasetiawan, F.; Gunnarsson, O. TheGWmethod. *Rep. Prog. Phys.* **1998**, *61*, 237−312.

(3) Reining, L. The GW Approximation: Content, Successes and Limitations: The GW Approximation. *Wiley Interdiscip. Rev.: Comput. Mol. Sci.* **2017**, *8*, No. e1344.

(4) Golze, D.; Dvorak, M.; Rinke, P. The GW Compendium: A Practical Guide to Theoretical Photoemission Spectroscopy. *Front. Chem.* **2019**, *7*, No. e377.

(5) Stan, A.; Dahlen, N. E.; Leeuwen, R. v. Fully Self-Consistent *GW* Calculations for Atoms and Molecules. *Europhys. Lett.* **2006**, *76*, 298−304.
(6) Stan, A.; Dahlen, N. E.; van Leeuwen, R. Levels of Self-Consistency in the GW Approximation. *J. Chem. Phys.* **2009**, *130*, 114105.
(7) Rostgaard, C.; Jacobsen, K. W.; Thygesen, K. S. Fully Self-Consistent GW Calculations for Molecules. *Phys. Rev. B: Condens. Matter Mater. Phys.* **2010**, *81*, 085103.
(8) Caruso, F.; Rinke, P.; Ren, X.; Scheffler, M.; Rubio, A. Unified Description of Ground and Excited States of Finite Systems: The Self-Consistent G W Approach. *Phys. Rev. B: Condens. Matter Mater. Phys.* **2012**, *86*, 081102.
(9) Caruso, F.; Rohr, D. R.; Hellgren, M.; Ren, X.; Rinke, P.; Rubio, A.; Scheffler, M. Bond Breaking and Bond Formation: How Electron Correlation Is Captured in Many-Body Perturbation Theory and Density-Functional Theory. *Phys. Rev. Lett.* **2013**, *110*, 146403.
(10) Caruso, F.; Rinke, P.; Ren, X.; Rubio, A.; Scheffler, M. Self-Consistent G W : All-Electron Implementation with Localized Basis Functions. *Phys. Rev. B: Condens. Matter Mater. Phys.* **2013**, *88*, 075105.
(11) Caruso, F. *Self-Consistent GW Approach for the Unified Description of Ground and Excited States of Finite Systems. PhD Thesis*; Freie Universität Berlin, 2013.
(12) Koval, P.; Foerster, D.; Sánchez-Portal, D. Fully Self-Consistent G W and Quasiparticle Self-Consistent G W for Molecules. *Phys. Rev. B: Condens. Matter Mater. Phys.* **2014**, *89*, 155417.
(13) Wilhelm, J.; Golze, D.; Talirz, L.; Hutter, J.; Pignedoli, C. A. Toward *GW* Calculations on Thousands of Atoms. *J. Phys. Chem. Lett.* **2018**, *9*, 306−312.
(14) Hybertsen, M. S.; Louie, S. G. First-Principles Theory of Quasiparticles: Calculation of Band Gaps in Semiconductors and Insulators. *Phys. Rev. Lett.* **1985**, *55*, 1418−1421.
(15) van Setten, M. J.; Weigend, F.; Evers, F. TheGW-Method for Quantum Chemistry Applications: Theory and Implementation. *J. Chem. Theory Comput.* **2013**, *9*, 232−246.
(16) Bruneval, F. Ionization Energy of Atoms Obtained from *GW* Self-Energy or from Random Phase Approximation Total Energies. *J. Chem. Phys.* **2012**, *136*, 194107.
(17) Bruneval, F.; Marques, M. A. L. Benchmarking the Starting Points of the *GW* Approximation for Molecules. *J. Chem. Theory Comput.* **2013**, *9*, 324−329.
(18) van Setten, M. J.; Caruso, F.; Sharifzadeh, S.; Ren, X.; Scheffler, M.; Liu, F.; Lischner, J.; Lin, L.; Deslippe, J. R.; Louie, S. G.; Yang, C.; Weigend, F.; Neaton, J. B.; Evers, F.; Rinke, P. GW100: Benchmarking G0W0 for Molecular Systems. *J. Chem. Theory Comput.* **2015**, *11*, 5665−5687.
(19) van Setten, M. J.; Costa, R.; Viñes, F.; Illas, F. Assessing *GW* Approaches for Predicting Core Level Binding Energies. *J. Chem. Theory Comput.* **2018**, *14*, 877−883.
(20) Hybertsen, M. S.; Louie, S. G. Electron Correlation in Semiconductors and Insulators: Band Gaps and Quasiparticle Energies. *Phys. Rev. B: Condens. Matter Mater. Phys.* **1986**, *34*, 5390−5413.
(21) Shishkin, M.; Kresse, G. Self-Consistent G W Calculations for Semiconductors and Insulators. *Phys. Rev. B: Condens. Matter Mater. Phys.* **2007**, *75*, 235102.
(22) Blase, X.; Attaccalite, C.; Olevano, V. First-Principles GW Calculations for Fullerenes, Porphyrins, Phtalocyanine, and Other Molecules of Interest for Organic Photovoltaic Applications. *Phys. Rev. B: Condens. Matter Mater. Phys.* **2011**, *83*, 115103.
(23) Faber, C.; Attaccalite, C.; Olevano, V.; Runge, E.; Blase, X. First-Principles GW Calculations for DNA and RNA Nucleobases. *Phys. Rev. B: Condens. Matter Mater. Phys.* **2011**, *83*, 115123.
(24) Faleev, S. V.; van Schilfgaarde, M.; Kotani, T. All-Electron Self-Consistent G W Approximation: Application to Si, MnO, and NiO. *Phys. Rev. Lett.* **2004**, *93*, 126406.
(25) van Schilfgaarde, M.; Kotani, T.; Faleev, S. Quasiparticle self-consistent GW theory. *Phys. Rev. Lett.* **2006**, *96*, 226402.
(26) Kotani, T.; van Schilfgaarde, M.; Faleev, S. V. Quasiparticle Self-Consistent G W Method: A Basis for the Independent-Particle Approximation. *Phys. Rev. B: Condens. Matter Mater. Phys.* **2007**, *76*, 165106.
(27) Ke, S.-H. All-Electron G W Methods Implemented in Molecular Orbital Space: Ionization Energy and Electron Affinity of Conjugated Molecules. *Phys. Rev. B: Condens. Matter Mater. Phys.* **2011**, *84*, 205415.
(28) Kaplan, F.; Harding, M. E.; Seiler, C.; Weigend, F.; Evers, F.; van Setten, M. J. Quasi-Particle Self-Consistent *GW* for Molecules. *J. Chem. Theory Comput.* **2016**, *12*, 2528−2541.
(29) Rangel, T.; Hamed, S. M.; Bruneval, F.; Neaton, J. B. Evaluating the GW Approximation with CCSD(T) for Charged Excitations Across the Oligoacenes. *J. Chem. Theory Comput.* **2016**, *12*, 2834−2842.
(30) Caruso, F.; Dauth, M.; van Setten, M. J.; Rinke, P. Benchmark of GW Approaches for the GW100 Test Set. *J. Chem. Theory Comput.* **2016**, *12*, 5076.
(31) Romaniello, P.; Guyot, S.; Reining, L. The Self-Energy beyond GW: Local and Nonlocal Vertex Corrections. *J. Chem. Phys.* **2009**, *131*, 154111.
(32) Romaniello, P.; Bechstedt, F.; Reining, L. Beyond the G W Approximation: Combining Correlation Channels. *Phys. Rev. B: Condens. Matter Mater. Phys.* **2012**, *85*, 155131.
(33) Berger, J. A.; Romaniello, P.; Tandetzky, F.; Mendoza, B. S.; Brouder, C.; Reining, L. Solution to the Many-Body Problem in One Point. *New J. Phys.* **2014**, *16*, 113025.
(34) Stan, A.; Romaniello, P.; Rigamonti, S.; Reining, L.; Berger, J. A. Unphysical and physical solutions in many-body theories: from weak to strong correlation. *New J. Phys.* **2015**, *17*, 093045.
(35) Di Sabatino, S.; Berger, J. A.; Reining, L.; Romaniello, P. Reduced density-matrix functional theory: Correlation and spectroscopy. *J. Chem. Phys.* **2015**, *143*, 024108.
(36) Di Sabatino, S.; Berger, J. A.; Reining, L.; Romaniello, P. Photoemission Spectra from Reduced Density Matrices: The Band Gap in Strongly Correlated Systems. *Phys. Rev. B* **2016**, *94*, 155141.
(37) Tarantino, W.; Romaniello, P.; Berger, J. A.; Reining, L. Self-Consistent Dyson Equation and Self-Energy Functionals: An Analysis and Illustration on the Example of the Hubbard Atom. *Phys. Rev. B* **2017**, *96*, 045124.
(38) Tarantino, W.; Mendoza, B. S.; Romaniello, P.; Berger, J. A.; Reining, L. Many-body perturbation theory and non-perturbative approaches: screened interaction as the key ingredient. *J. Phys.: Condens. Matter* **2018**, *30*, 135602.
(39) Di Sabatino, S.; Koskelo, J.; Berger, J. A.; Romaniello, P. Is paramagnetic FeO strongly correlated. **2020**, arXiv:2002.11198.
(40) Loos, P.-F.; Romaniello, P.; Berger, J. A. Green functions and self-consistency: insights from the spherium model. *J. Chem. Theory Comput.* **2018**, *14*, 3071−3082.
(41) Véril, M.; Romaniello, P.; Berger, J. A.; Loos, P.-F. Unphysical Discontinuities inGWMethods. *J. Chem. Theory Comput.* **2018**, *14*, 5220−5228.
(42) Golze, D.; Keller, L.; Rinke, P. Accurate Absolute and Relative Core-Level Binding Energies from GW. *J. Phys. Chem. Lett.* **2020**, *11*, 1840−1847.
(43) Loos, P.-F.; Scemama, A.; Duchemin, I.; Jacquemin, D.; Blase, X. Pros and Cons of the Bethe−Salpeter Formalism for Ground-State Energies. *J. Phys. Chem. Lett.* **2020**, *11*, 3536−3545.
(44) Langreth, D. C.; Perdew, J. P. The gradient approximation to the exchange-correlation energy functional: A generalization that works. *Solid State Commun.* **1979**, *31*, 567−571.
(45) Gunnarsson, O.; Lundqvist, B. I. Exchange and correlation in atoms, molecules, and solids by the spin-density-functional formalism. *Phys. Rev. B: Solid State* **1976**, *13*, 4274−4298.
(46) Furche, F.; Van Voorhis, T. Fluctuation-dissipation theorem density-functional theory. *J. Chem. Phys.* **2005**, *122*, 164106.
(47) Toulouse, J.; Gerber, I. C.; Jansen, G.; Savin, A.; Angyan, J. G. Adiabatic-Connection Fluctuation-Dissipation Density-Functional

https://dx.doi.org/10.1021/acs.jctc.0c00896
J. Chem. Theory Comput. 2021, 17, 191−200

Theory Based on Range Separation. *Phys. Rev. Lett.* **2009**, *102*, 096404. DOI: 10.1103/physrevlett.102.096404
(48) Toulouse, J.; Zhu, W.; Angyan, J. G.; Savin, A. Range-Separated Density-Functional Theory With the Random-Phase Approximation: Detailed Formalism and Illustrative Applications. *Phys. Rev. A: At., Mol., Opt. Phys.* **2010**, *82*, 032502. DOI: 10.1103/physreva.82.032502
(49) Ángyán, J. G.; Liu, R.-F.; Toulouse, J.; Jansen, G. Correlation Energy Expressions from the Adiabatic-Connection Fluctuation Dissipation Theorem Approach. *J. Chem. Theory Comput.* **2011**, *7*, 3116−3130.
(50) Olsen, T.; Thygesen, K. S. Static Correlation Beyond the Random Phase Approximation: Dissociating H2 With the Bethe-Salpeter Equation and Time-Dependent GW. *J. Chem. Phys.* **2014**, *140*, 164116.
(51) Maggio, E.; Kresse, G. Correlation Energy for the Homogeneous Electron Gas: Exact Bethe-Salpeter Solution and an Approximate Evaluation. *Phys. Rev. B* **2016**, *93*, 235113.
(52) Holzer, C.; Gui, X.; Harding, M. E.; Kresse, G.; Helgaker, T.; Klopper, W. Bethe-Salpeter correlation energies of atoms and molecules. *J. Chem. Phys.* **2018**, *149*, 144106.
(53) Li, J.; Drummond, N. D.; Schuck, P.; Olevano, V. Comparing Many-Body Approaches Against the Helium Atom Exact Solution. *SciPost Phys.* **2019**, *6*, 040.
(54) Li, J.; Duchemin, I.; Blase, X.; Olevano, V. Ground-state correlation energy of beryllium dimer by the Bethe-Salpeter equation. *SciPost Phys.* **2020**, *8*, 20.
(55) Salpeter, E. E.; Bethe, H. A. A Relativistic Equation for Bound-State Problems. *Phys. Rev.* **1951**, *84*, 1232.
(56) Strinati, G. Application of the Green's functions method to the study of the optical properties of semiconductors. *Riv. Nuovo Cimento* **1988**, *11*, 1−86.
(57) Blase, X.; Duchemin, I.; Jacquemin, D. The Bethe-Salpeter equation in chemistry: relations with TD-DFT, applications and challenges. *Chem. Soc. Rev.* **2018**, *47*, 1022−1043.
(58) Blase, X.; Duchemin, I.; Jacquemin, D.; Loos, P.-F. The Bethe-Salpeter Equation Formalism: From Physics to Chemistry. *J. Phys. Chem. Lett.* **2020**, *11*, 7371.
(59) Hedin, L. On correlation effects in electron spectroscopies and theGWapproximation. *J. Phys.: Condens. Matter* **1999**, *11*, R489−R528.
(60) Bruneval, F.; Vast, N.; Reining, L. Effect of self-consistency on quasiparticles in solids. *Phys. Rev. B: Condens. Matter Mater. Phys.* **2006**, *74*, 045102.
(61) Gatti, M.; Bruneval, F.; Olevano, V.; Reining, L. Understanding Correlations in Vanadium Dioxide from First Principles. *Phys. Rev. Lett.* **2007**, *99*, 266402.
(62) Vidal, J.; Trani, F.; Bruneval, F.; Marques, M. A. L.; Botti, S. Effects of Electronic and Lattice Polarization on the Band Structure of Delafossite Transparent Conductive Oxides. *Phys. Rev. Lett.* **2010**, *104*, 136401.
(63) Rangel, T.; Kecik, D.; Trevisanutto, P. E.; Rignanese, G.-M.; Van Swygenhoven, H.; Olevano, V. Band structure of gold from many-body perturbation theory. *Phys. Rev. B: Condens. Matter Mater. Phys.* **2012**, *86*, 125125.
(64) Tanwar, A.; Fabiano, E.; Trevisanutto, P. E.; Chiodo, L.; Della Sala, F. Accurate ionization potential of gold anionic clusters from density functional theory and many-body perturbation theory. *Eur. Phys. J. B* **2013**, *86*, 161.
(65) Boulanger, P.; Jacquemin, D.; Duchemin, I.; Blase, X. Fast and Accurate Electronic Excitations in Cyanines with the Many-Body Bethe-Salpeter Approach. *J. Chem. Theory Comput.* **2014**, *10*, 1212−1218.
(66) Knight, J. W.; Wang, X.; Gallandi, L.; Dolgounitcheva, O.; Ren, X.; Ortiz, J. V.; Rinke, P.; Körzdörfer, T.; Marom, N. Accurate Ionization Potentials and Electron Affinities of Acceptor Molecules III: A Benchmark of *GW* Methods. *J. Chem. Theory Comput.* **2016**, *12*, 615−626.
(67) Li, J.; D'Avino, G.; Duchemin, I.; Beljonne, D.; Blase, X. Combining the Many-Body GW Formalism with Classical Polarizable Models: Insights on the Electronic Structure of Molecular Solids. *J. Phys. Chem. Lett.* **2016**, *7*, 2814−2820.
(68) Fujita, T.; Noguchi, Y. Development of the fragment-based COHSEX method for large and complex molecular systems. *Phys. Rev. B* **2018**, *98*, 205140.
(69) Faber, C.; Boulanger, P.; Attaccalite, C.; Cannuccia, E.; Duchemin, I.; Deutsch, T.; Blase, X. Exploring approximations to the *GW* self-energy ionic gradients. *Phys. Rev. B: Condens. Matter Mater. Phys.* **2015**, *91*, 155109.
(70) Kang, W.; Hybertsen, M. S. Enhanced static approximation to the electron self-energy operator for efficient calculation of quasiparticle energies. *Phys. Rev. B: Condens. Matter Mater. Phys.* **2010**, *82*, 195108.
(71) Hesselmann, A.; Gorling, A. Random-Phase Approximation Correlation Methods for Molecules and Solids. *Mol. Phys.* **2011**, *109*, 2473.
(72) Colonna, N.; Hellgren, M.; de Gironcoli, S. Correlation Energy Within Exact-Exchange Adiabatic Connection Fluctuation-Dissipation Theory: Systematic Development and Simple Approximations. *Phys. Rev. B: Condens. Matter Mater. Phys.* **2014**, *90*, 125150.
(73) Loos, P. F. *QuAcK: A Software for Emerging Quantum Electronic Structure Methods*. https://github.com/pfloos/QuAcK.
(74) Bruneval, F.; Rangel, T.; Hamed, S. M.; Shao, M.; Yang, C.; Neaton, J. B. Molgw 1: Many-Body Perturbation Theory Software for Atoms, Molecules, and Clusters. *Comput. Phys. Commun.* **2016**, *208*, 149−161.
(75) Pulay, P. Convergence Acceleration of Iterative Sequences. the Case of Scf Iteration. *Chem. Phys. Lett.* **1980**, *73*, 393−398.
(76) Pulay, P. ImprovedSCF Convergence Acceleration. *J. Comput. Chem.* **1982**, *3*, 556−560.
(77) Berger, J. A.; Reining, L.; Sottile, F. *Ab Initio* Calculations of Electronic Excitations: Collapsing Spectral Sums. *Phys. Rev. B: Condens. Matter Mater. Phys.* **2010**, *82*, 041103.
(78) Berger, J. A.; Reining, L.; Sottile, F. Efficient G W Calculations for SnO 2 , ZnO, and Rubrene: The Effective-Energy Technique. *Phys. Rev. B: Condens. Matter Mater. Phys.* **2012**, *85*, 085126.
(79) Berger, J. A.; Reining, L.; Sottile, F. Efficient calculation of the polarizability: a simplified effective-energy technique. *Eur. Phys. J. B* **2012**, *85*, 326.
(80) Duchemin, I.; Blase, X. Separable resolution-of-the-identity with all-electron Gaussian bases: Application to cubic-scaling RPA. *J. Chem. Phys.* **2019**, *150*, 174120.
(81) Duchemin, I.; Blase, X. Robust Analytic-Continuation Approach to Many-Body GW Calculations. *J. Chem. Theory Comput.* **2020**, *16*, 1742−1756.
(82) Christiansen, O.; Koch, H.; Jørgensen, P. The second-order approximate coupled cluster singles and doubles model CC2. *Chem. Phys. Lett.* **1995**, *243*, 409−418.
(83) Purvis, G. D.; Bartlett, R. J. A full coupled-cluster singles and doubles model: The inclusion of disconnected triples. *J. Chem. Phys.* **1982**, *76*, 1910−1918.
(84) Christiansen, O.; Koch, H.; Jo/rgensen, P. Response functions in the CC3 iterative triple excitation model. *J. Chem. Phys.* **1995**, *103*, 7429−7441.
(85) Huber, K. P.; Herzberg, G. *Molecular Spectra and Molecular Structure: IV. Constants of Diatomic Molecules*; van Nostrand Reinhold Company, 1979.
(86) Krause, K.; Harding, M. E.; Klopper, W. Coupled-Cluster Reference Values For The Gw27 And Gw100 Test Sets For The Assessment Of Gw Methods. *Mol. Phys.* **2015**, *113*, 1952.